Journal of Thermal Analysis and Calorimetry (2021) 146:1593–1601
https://doi.org/10.1007/s10973-020-10181-4

The hydration properties of ultra-fine ground granulated blast-furnace slag cement with a low water-to-binder ratio

Yuqi Zhou[1,2] · **Zengqi Zhang**[2]

Received: 28 June 2019 / Accepted: 11 August 2020 / Published online: 28 August 2020

Abstract
Based on the fundamental principles of preparing reactive powder concrete (RPC), a new type of RPC was composed by replacing cement with the active powder component ultra-fine ground granulated blast-furnace slag (GGBS). GGBS is proposed as a potential alternative to silica fume (SF), which is currently the most commonly used RPC mineral admixture. In order to improve the brittleness of RPC, a steel fibre with appropriate length/diameter ratio was added. The ultra-fine GGBS (UFS) or SF replacement level was 20% by mass, with a water-to-binder (*w*/*b*) ratio of 0.18. The concrete specimens were pre-cured for 6 h at 20 °C and then exposed to steam curing conditions for 3 days. This study investigates the effects of the UFS and the SF on the durability of the RPC by examining the hydration properties, mechanical properties and permeability of RPC. Test results reveal that replacing the cement with UFS or SF does have a significant effect on the hydration properties, our results indicate that the inclusion of SF or UFS can accelerate the early hydration of cement and increase the consumption of $Ca(OH)_2$. The mercury porosimetry and chloride ion penetration tests results revealed that RPC has a very low porosity and very dense structure. RPC with the addition of steel fibre exhibited a higher compressive strength than the RPC without steel fibre. Incorporating UFS into RPC had similar advantages to incorporating SF, but UFS proved to be the more economical admixture.

Keywords Ultra-fine GGBS · Silica fume · Steel fibre · Reactive powder concrete · Hydration properties

Introduction

As the Chinese social economy develops, the demand for both long-lasting and functional building structures has grown, with current construction trends gravitating towards building materials which possess both ultra-high strength and durability. This increases the requirements for the mechanical properties and the resilience of concrete [1–4], leading to the development and application of high performance concrete (HPC) and ultra-high-performance concrete (UHPC) [5, 6]. The toughness of UHPC has been further improved with the addition of steel fibres, resulting in a type of concrete called ultra-high-performance fibre-reinforced concrete (UHPFRC) [7–9]. Based on research conducted by Richard et al. [10], a new type of UHPC was developed, dubbed reactive powder concrete (RPC) due to the incorporation of high-activity volcanic ash material and the replacement of coarse aggregate with fine quartz sand (with a particle size less than 0.6 mm) or steel aggregate (with a particle size less than 0.8 mm). RPC is developed through microstructural enhancement techniques and is characterized by its super-high strength, extreme durability, excellent volume stability and superior toughness [11, 12]. RPC with these superior qualities has been applied extensively in civil, petroleum, nuclear power, municipal, marine and military facilities, as well as in other projects [13]. However, the water-to-binder ratio of conventional RPC tends to be low and, for practical engineering, steel fibre must be added to improve its toughness, thereby increasing the difficulty of mixing and moulding the material. This increase in RPC's production costs has hindered its promotion and application.

Silica fume (SF) is the most commonly used of the RPC mineral admixtures due to its high activity and particle filling effects, properties which play an important role in ensuring RPC strength [14, 15]. Using SF improves RPC

✉ Zengqi Zhang
zzq2019@mail.tsinghua.edu.cn

1 China Construction First Group Construction and Development Co., Ltd., Beijing 100102, China

2 Department of Civil Engineering, Tsinghua University, Beijing 100084, China

in three key ways. The first is its particle filling effect [16]; due to the very small mean particle size of SF it can easily fill pores between particles, thereby increasing the density of the pastes and improving the overall strength of RPC. The second effect is morphological [17, 18]; as the SF particles possess glassy and spherical characteristics, which can provide 'ball-bearing' effect and decrease the flow resistance of the mixture, thus improving the rheology of RPC. The final effect is pozzolanic [19]; as the secondary hydration products fill the interior of the concrete, these block the interconnected pores, inhibiting ion transportation and enhancing durability. However, the proportion of cement in conventional RPC is generally high, and the SF content is often over 25% (determined by the mass of cement) which not only increases production costs but also negatively influences the hydration heat and may lead to shrinkage problems. Replacing both cement and SF with other mineral admixtures appears to be a feasible solution to these problems.

Ground granulated blast-furnace slag (GGBS) is a by-product from molten slag discharged, when iron is smelted using a rapid water-quenching technique. GGBS has been used in the cement and concrete industry for many years [20]. As a mineral admixture, GGBS can improve both fresh and hardened concrete by increasing workability, retarding the bleeding of fresh concrete, decreasing the heat of hydration, improving long-term strength and corrosion resistance and reducing porosity and permeability [21, 22]. In addition, the price of GGBS is lower than SF, making it a more economical choice than the SF-blended concrete. In contrast to normal GGBS, ultra-fine GGBS (UFS) has an increased surface area, which increases both the hydration rates and the number of pozzolanic reactions and improves its filling abilities [23]. The advantages of UFS are numerous and include reducing the total pore volume, reducing pore connections and an improved filling of pores within the interfacial transition zone (ITZ), which can accelerate the rate of strength development, reduce permeability, and improve the overall durability of the RPC.

In this investigation, the RPC was prepared with a low water-to-binder (*w*/*b*) ratio of 0.18. The cementitious materials that replaced ordinary Portland cement (OPC) were UFS and SF. In addition, in order to improve the brittleness of RPC, a steel fibre with an appropriate length/diameter ratio was added. We compared the effects of using SF and UFS in RPC by examining a number of criteria, including early hydration, pore structure, compressive strength, and resistance to chloride ion permeability. It is expected that our results will help create a scientific basis for using UFS in the preparation of RPC.

Experimental

Raw material

Ordinary Portland Cement (OPC, China Building Materials Academy Co., Ltd.) complies with the Chinese Standards GB175-2007 and has a Blaine fineness of 341 m^2/kg. The mineral admixtures (MA) used were SF (SLT comprehensive utilization of resources Co., Ltd.) with a nitrogen BET surface area of 17,650 m^2/kg, and two ultra-fine GGBS (UFS, Wuhan VCEM Technology Development Co., Ltd.) admixtures, one with a nitrogen BET surface area of 2435 $m^2\ kg^{-1}$ (UFS1) and the other of 3955 $m^2\ kg^{-1}$ (UFS2). The SF and UFS used in this work were commercially available materials. The detailed chemical compositions of OPC, SF, UFS1, and UFS2 are shown in Table 1. The XRD patterns are shown in Fig. 1. The steel fibre had a diameter of 0.18–0.22 mm and a length of 12–14 mm. Fine quartz sand with a particle size of 0.315–0.63 mm and coarse quartz sand with a particle size of 0.63–1.25 mm were used. A polycarboxylate superplasticizer (PS) was also used to adjust the concrete's fluidity.

Mix proportions

The mass replacement of MA to cement was fixed at 20% with a low water-to-binder (*w*/*b*) ratio of 0.18. The mix proportions of pastes and concretes are shown in Tables 2 and 3, respectively. Plain cement samples (C) were used as the reference samples. The samples containing SF, UFS1 and UFS2 are referred to as S, U1 and U2, respectively. The concrete samples containing the additional steel fibre are referred to as C#, S#, U1# and U2#, respectively.

Table 1 Chemical composition and surface area of OPC, SF, UFS1 and UFS2

Name	Composition/%			
	OPC	SF	UFS1	UFS2
CaO	67.8	0.17	43.0	43.0
SiO_2	18.1	97.34	32.3	32.3
Al_2O_3	4.3	0.34	14.3	14.4
MgO	1.95	0.27	7.0	6.9
SO_3	3.08	0.77	1.0	1.0
Fe_2O_3	3.3	0.06	0.3	0.2
Na_2O	0.17	0.11	0.2	0.2
K_2O	0.68	0.82	0.5	0.5
Surface area/$m^2\ kg^{-1}$	341	17,650	2435	3955

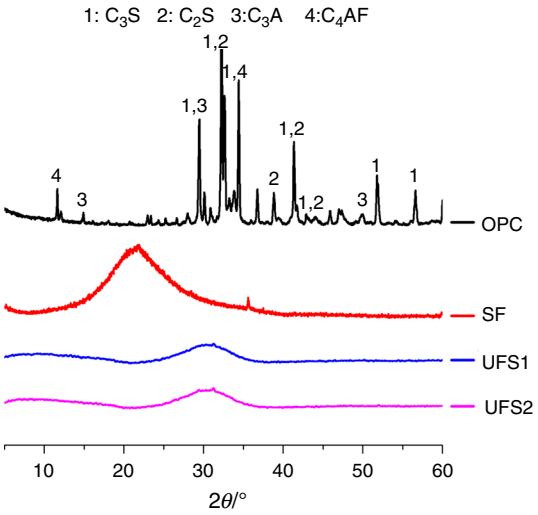

Fig. 1 The XRD patterns of OPC, SF, UFS1 and UFS2

Table 2 Mix proportions of pastes

Samples	By mass/%				Water-to-binder ratio
	OPC	SF	UFS1	UFS2	
C	100				0.18
S	80	20			0.18
U1	80		20		0.18
U2	80			20	0.18

Specimen preparation

The mixing method should ensure the homogenization of the RPC specimens. All RPC specimens were prepared according to the GB/T 31387-2015, 'Reactive powder concrete' [24], as following procedures: (1) The feeding process is in order of quartz sands, steel fibre, cement and MA. These dry mixtures are pre-mixed for 4 min. (2) Addition of the volume of water containing the superplasticizer and mixing for 5 min. (3) Fresh mixed RPC was then poured in 100 mm × 100 mm × 100 mm moulds and compacted to remove air voids using a vibrating for 30 s. (4) The RPC specimens were covered by plastic sheets for the next curing process.

Curing process

Two groups of each specimen (listed in Tables 2, 3) were prepared and then pre-cured for 6 h at normal temperature (20 °C) prior to steam curing. After pre-curing, the specimens were exposed to steam curing conditions for 3 days. First, the specimens were steam cured at (40 ± 5) °C for 1 day. After the steam curing, all of the specimens were cooled to room temperature and then de-moulded, and followed by 2 days steam curing at (70 ± 5) °C. One group of the concrete samples was taken directly to the experimental area following the steam curing. (These samples were 3 days old.) The other group remained under the standard curing conditions until the concrete samples reached an age of 14 days.

Test methods

The heat evolution of the four mixture samples was measured using a TAM Air Calorimeter at 25 °C and 50 °C within 72 h, respectively. The mix proportions of these samples are shown in order in Table 2. These results indicate the early hydration activity of the samples.

Two groups of each specimen (listed in Table 2) were prepared and cured to the ages of 3 and 14 days, respectively. The hardened pastes were extracted once they had reached the chosen testing age and then immersed in absolute alcohol to prevent further hydration. The samples were dried in an electric vacuum drying oven before undergoing testing. Thermogravimetric (TG) analysis, mercury intrusion porosimetry (MIP) and X-ray diffraction (XRD) tests were performed on theses dried samples, respectively.

The TG analysis was conducted using a simultaneous thermal analyser with a uniform heating rate of 10 °C per

Table 3 Mix proportions of concretes/(kg m^{-3})

Samples	OPC	SF	UFS1	UFS2	Steel fibre	Water	Fine quartz sands	Coarse quartz sands
C	916					165	760	410
S	732.8	183.2				165	760	410
U1	732.8		182.3			165	760	410
U2	732.8			182.3		165	760	410
C-#	916				100	165	760	410
S-#	732.8	183.2			100	165	760	410
U1-#	732.8		182.3		100	165	760	410
U2-#	732.8			182.3	100	165	760	410

minute from room temperature to 900 °C, using platinum crucibles with approximately 0.004 g of sample under a nitrogen flow. The calcium hydroxide (CH) content of the hydration products was calculated based on the TG/DTG curves of the hardened paste samples at the respective ages of 3 and 14 days, respectively.

MIP with an operating pressure up to 60,000 lb in^{-2} (about 413.76 MPa) was used to determine the pore size and distribution of the hardened paste samples at the ages of 3 and 14 days, respectively.

XRD was used to determinate the mineral phases of the hardened pastes' hydration products following the steam curing at an age of 3 days. An internal standard of 20 mass% of SiO_2 was mixed manually with the samples in an agate mortar for 20 min to obtain a good homogeneity. XRD patterns were acquired by X-ray diffraction analyzer with D/MAX-RB models of target X-ray diffraction, using copper cathode and continuous scan. The test data were collected from the 2θ range of 5° to 65° on the continuous mode and were analysed using JADE software. Rietveld methodology was used to calculate the CH content of the samples.

Each RPC concrete specimen, C, S, U1 and U2 (without steel fibre); C-#, S-#, U1-# and U2-# (with steel fibre) was prepared for the compressive strength tests, where each value is averaged from the results of three cubes.

The chloride ion permeability of the concretes (without steel fibre) was tested at an age of 14 days by measuring a current passing through the concrete. These results were evaluated according to ASTM C1202 [25] 'Standard Test Method for Electrical Indication of Concretes Ability to Resist Chloride Ion Penetration'.

Results and discussion

Hydration heat

Figure 2a, b shows the exothermic rate and cumulative hydration heat of cementitious materials at 25 °C, respectively. As shown in Fig. 2a, the second peak in the sample containing SF (S) appeared significantly earlier than in the plain cement sample (C). This is due to the ultra fineness of SF, which can cause a nucleation that promotes the hydration of cement. In addition, SF has a large specific surface area and a high reactivity, which can accelerate its pozzolanic reactivity. Hence, the replacement of cement with SF can accelerate the early hydration process and advance the second exothermic peak. In general, the activity of ordinary GGBS is much lower than that of cement, and thus the second exothermic peak should be slightly delayed than in a cement-GGBS system. However, as shown in Fig. 2a, the replacement of cement with ultra-fine GGBS (UFS) can make the second exothermic peak appear first, almost at the same time as the plain cement sample. In theory, grinding

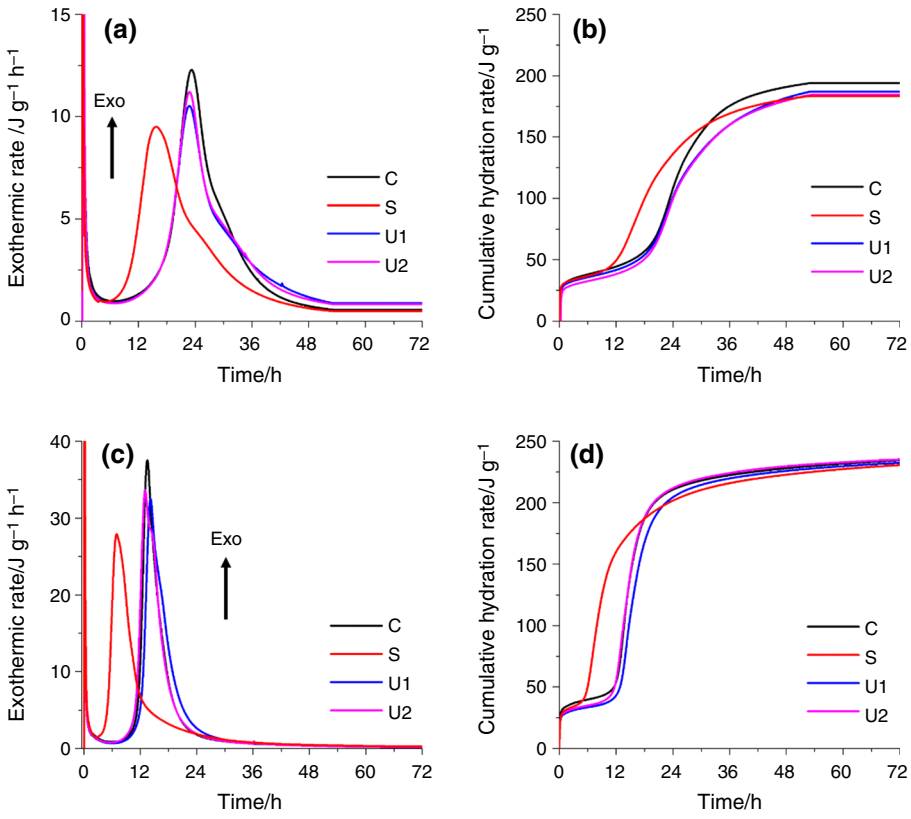

Fig. 2 **a** Exothermic rate curves and **b** Cumulative heat curves of binders during hydration at 25 °C; **c** Exothermic rate curves and **d** Cumulative heat curves of binders during hydration at 50 °C

the ordinary GGBS into a finer powder and thereby creating a larger specific surface area could improve the nucleating effect and accelerate the hydration reaction [26]. In addition, the peak intensities of the UFS-cement system (U1 and U2) were lower than those of the plain cement samples. This is because of the decrease in cement content and the ultra fineness of UFS, which lead to greater water absorption and a reduction in the cement's hydration. When the cement was replaced with UFS1 or UFS2 it underwent a very similar hydration process, but did exhibit differences in terms of peak intensity. U2 displayed a slightly higher peak intensity than U1, which may be due to the already minute particle size of UFS1, meaning that further grinding has very little effect on the hydration of the cement. Meanwhile, the sample containing SF exhibited the lowest peak intensity. This may be caused by the pelletization or densification of the SF agglomerates [27], where the small individual particles gather into relatively large clumps—a process which adversely effects the functionality of SF [28].

As shown in Fig. 2b, during early-stage hydration, the cumulative heat of the sample containing SF was obviously higher than that of the plain cement sample, while, the samples containing UFS were very close to that of plain cement sample. These results are consistent with the results of exothermic rate. However, the finally total cumulative heat shows the order is $C > U1 \approx U2 > S$. The reasons are maybe due to the early reaction of the sample containing SF was too fast and the hydration products were not evenly distributed which may adhere to the surface of the unhydrated particles [29, 30]. Therefore, the subsequent reaction of SF-cement system would be inhibited, so that reduced the finally total cumulative heat. In addition, the cumulative heat curve of the sample containing UFS1 was almost coincided with that of UFS2. It shows again that the further grinding of UFS has little effect on the hydration of UFS-cement system.

Figure 2c, d shows the exothermic rates and cumulative hydration temperatures of the cementitious materials at 50 °C. As shown in Fig. 2c, when compared with the results at 25 °C, the main peaks shifted significantly to the left, and the peak intensity increased and the half-peak width decreased. These results indicate that the reaction process of these cementitious materials was accelerated at higher temperatures [31]. As shown in Fig. 2d, the final total cumulative heat results were as follows: $C \approx U2 \approx U1 \approx S$. Compared with Fig. 2b, the final total cumulative heat of all the blended samples have increased and the differences between them are not significant. The explanation can be that the reaction of SF and UFS is significantly stimulated by the high temperature and accelerate the dissolution rate of composite binders, which contributes to the hydration heat of the composite binder within 72 h at 50 °C. Furthermore, this indicates that the excitation effect produced by high temperatures was more effective for SF and UFS than for pure cement. In addition, the cumulative heat curve of the sample containing UFS2 almost coincided with that of the plain cement sample. This suggests that the excitation effect created by higher temperatures was more significant for UFS2 than for UFS1.

Thermogravimetric (TG) analysis

Figure 3a, b shows the hardened paste samples' TG and DTG curves at the ages of 3 and 14 days, respectively. As shown in the DTG curve, an endothermic peak occurred for each sample at approximately 300–500 °C, a result which corresponds with the decomposition of CH. The total amount of CH was then calculated based on the DTG curves as shown in Table 4, which presents the content of CH in the hardened paste samples at the ages of 3 and 14 days. The CH content of the samples containing SF, UFS1 or UFS2 was lower than that of the plain cement sample, additionally the decreased value was higher than the replacement level of 20%. This is due to the pozzolanic reaction of SF and UFS, which consumes CH within the cementitious system [32]. Moreover, steam curing at elevated temperatures can strongly activate SF and UFS, thereby increasing the reaction degree. However, the CH content of the SF sample was significantly lower than that of the UFS sample.

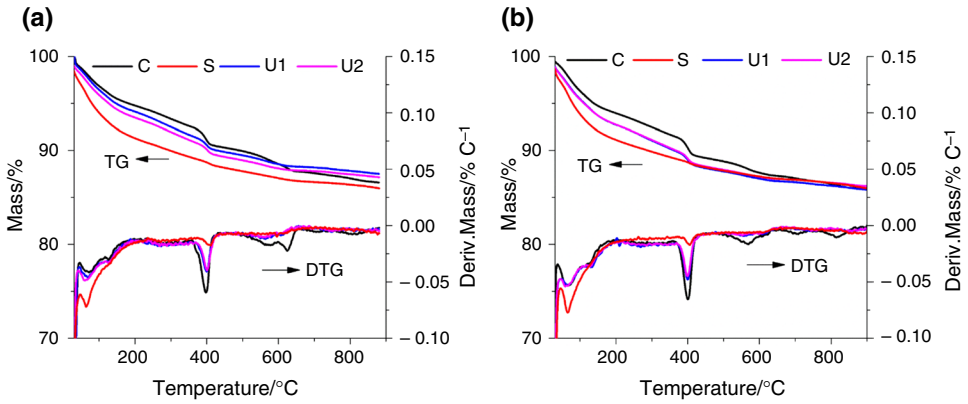

Fig. 3 TG/DTG curves of the hardened paste samples at the ages of **a** 3 and **b** 14 days

Table 4 The content of CH in the hardened paste samples at the ages of 3 and 14 days, respectively

Samples	CH content/%	
	3 days	14 days
C	7.73	8.96
S	2.18	1.93
U1	4.97	6.41
U2	4.89	6.25

This is because the content of calcium oxide (CaO) in the UFS (43%) is higher than that in the SF (0.17%) as shown in Table 1. Watcharapong [33] has reported that the CaO content plays a significant role in accelerates the precipitation of CH. Therefore, UFS can provide partial Ca^{2+} for the formation of CH, while the amount of CH consumed by the SF was almost entirely produced by cement hydration. In addition, the CH content of U1 and U2 did exhibit distinct differences due to there being the same amount of CaO in both UFS1 and UFS2.

The CH content of all the samples altered slightly over the period of 3 to 14 days. This indicates that the early steam curing significantly enhanced the reaction degree of these samples and further curing does little to improve the degree of reaction, and resulted in only marginal increases of CH content. It is interesting to note that the CH content of the sample containing SF decreased slightly over the 3 to 14 day range. This is because a large amount of CH was consumed in the SF-cement system during the early steam curing period and the extremely low levels of CaO in SF could not provide enough Ca^{2+} for the formation of CH.

Pore structure of the hardened pastes

The MIP test results are shown in Fig. 4. After steam curing for 3 days, the pore size distribution curves of the hardened pastes containing UFS1 (U1) and UFS2 (U2) were practically identical, and the pore structure was optimized compared with the plain cement as shown in Fig. 4a, c. This was caused by the UFS hydration reaction being activated during the process of steam curing, which meant that hydration products had filled some of the pores present in the hardened paste. In addition, the physical filling effect of UFS is able to alter the density of pore structure and decrease the total porosity. However, under the same dosage, the porosity of the hardened pastes containing SF (S) was larger than that of the hard pastes made of plain cement. This may be due to the partially undispersed SF agglomerates in the cement paste, as these SF agglomerations can hinder improvements in pore structure.

Figure 4b, d shows the pore size distribution curves of the hardened pastes samples under both the standard, 3 days curing condition and up to the age of 14 days. It can be seen that there was no significant improvement in the porosity in the hardened paste samples. This may be caused by the early

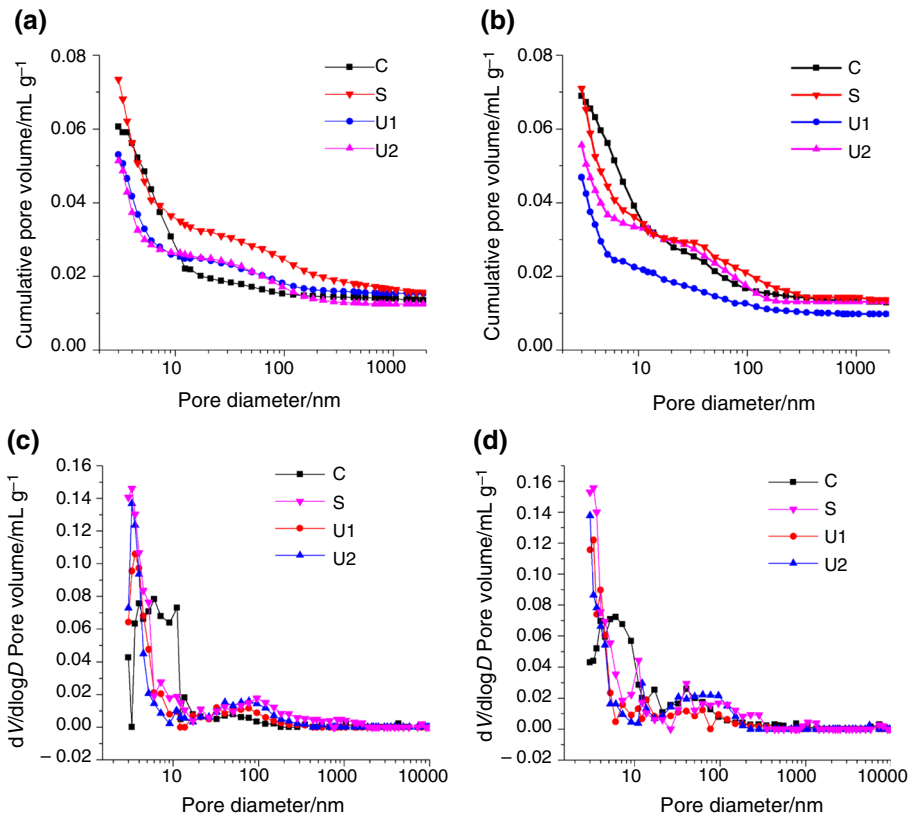

Fig. 4 Pore structures of the hardened paste samples at the ages of **a**, **c** 3 and **b**, **d** 14 days

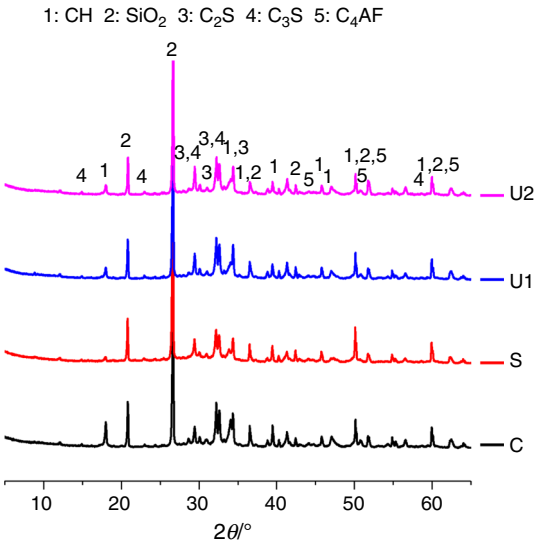

Fig. 5 XRD patterns of the hardened pastes C, S, U1 and U2 after steam curing

Table 5 Results of quantitative XRD (QXRD) analysis for the hardened pastes C, S, U1 and U2 after steam curing

Phase	Mass fraction-QXRD/mass%			
	C	S	U1	U2
CH	8.89	2.33	5.58	5.36

reaction of the samples, which occurred too quickly during the early steam curing process, thereby making the hydration products coarse and unevenly distributed in the matrix when subjected to further standard curing conditions. For this reason, it is easy to increase the porosity of the hardened pastes.

X-ray diffraction analysis

The XRD patterns for the hardened paste samples after steam curing (at an age of 3 days) are shown in Fig. 5. The formation of the hydration products is proved by the XRD results and all samples produced CH as hydration products. C_3A contained in cement were not identified in hardened pastes, while the C_2S, C_3S and C_4AF were identified as unreacted residual phases. Rietveld methodology was used to calculate the CH content present in samples. The results of the Rietveld quantitative XRD (QXRD) analysis for the samples are shown in Table 5. The XRD scans of the four hardened pastes were very similar, with the CH content of the four samples almost matching the results of the TG test (as shown in Table 4). As mentioned before, the CH content indicates changes in the hydration products that are generated by pozzolanic reactions caused by SF or UFS. Our QXRD results confirmed the higher consumption rate of CH, which contributed to the formation of strength possessing phases in the C-SF or C-UFS systems.

Compressive strength

Figure 6a, b shows the compressive strengths of the concrete cubes with and without steel fibre at the ages of 3 and 14 days, respectively. Based on the column figures below, the compressive strength of the concretes can be seen to increase with the addition of the steel fibres. This may be caused by the steel fibres intersecting with and arresting the microcracks that develop in the ITZ, thereby increasing the strength of concrete [34]. The SF and UFS concretes that contained steel fibres had a higher compressive strength than the control concretes. The addition of ultra-fine powder to the matrix improved the bond between the cement paste and the aggregate particles, as well as increasing the density of the cement paste. This, in turn, significantly improved the compressive strength of the concrete. It was noted that over the 3 to 14 day period, the compressive strength of concrete exhibited no obvious change. This indicates that the compressive strength of the concrete increased rapidly during the initial steam curing process.

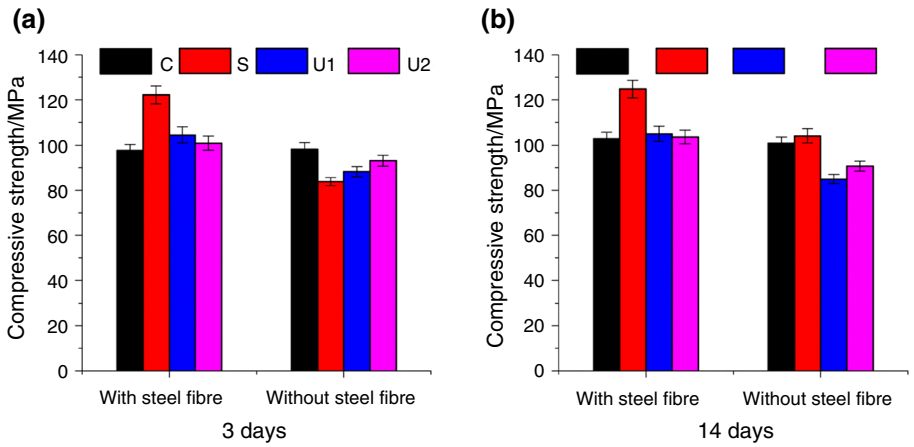

Fig. 6 Compressive strength of the concrete cubes with and without steel fibre at the ages of **a** 3 and **b** 14 days

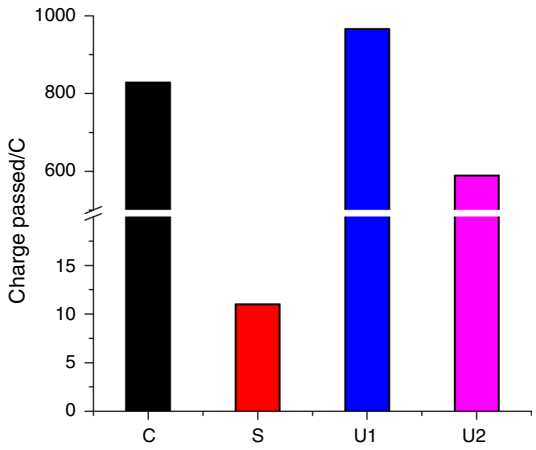

Fig. 7 The charge passed of the concrete samples without steel fibre at an age of 14 days

However, the SF and UFS concretes without steel fibre had lower compressive strength than the control concretes at 3 days. As shown in Fig. 2, the hydration degrees of SF and UFS composite binder are lower than plain cement at early hydration period, and the main contribution to compressive strength is the hydration of cement. Hence, the plain cement concrete without steel fibre shows highest compressive strength at 3 days. From 3 to 14 days, the compressive strength of the concrete displayed no obvious change except in sample S. This is because the secondary hydrated of SF at later hydration period and the filling effect of SF contributes to higher strength of RPC containing SF at an age of 14 days. It should be note that the higher compressive strength value is attributed to the incorporation of steel fibres in the RPCs. These results indicated that the presence of the steel fibre had a considerable effect on the mechanical properties of RPC.

Chloride ion permeability

The charge passed of the concrete samples without steel fibre at an age of 14 days is shown in Fig. 7. As reported, a reduction in chloride permeability indicates an improved resistance to chloride ion penetration. Figure 7 shows the chloride permeability grade of all of the RPC samples is at the 'Very Low' status, indicating that the RPC has good properties of the chloride resistance. When comparing the strength of the charge passing through OPC, SF, UFS1 and UFS2 RPC the results are as follows: S < U2 < C < U1. The improvement of microfiller in RPC by the ultra-fine powder and its higher secondary hydration levels contributes to blocking the connected pores, which is beneficial to improve the pore structure and the ITZ of RPC [35]. It should be noted that the amount of charge passing through the S sample was extremely low, which indicates that the inclusion of SF in RPC had a significant effect on chloride ion permeability. The pozzolanic reaction of SF consumes a large amount of CH (as shown in Fig. 3b), thus improving the ITZ, and the highest compressive strength of SF-RPC without steel fibres (as shown in Fig. 6b) shows the better compactness of concrete. Therefore, the RPC containing SF shows the best chloride ion permeability resistance.

Conclusions

The experimental results presented in this paper have verified that the incorporation of ultra-fine GGBS (UFS) in the RPC matrix can improve the hydration properties, the mechanical properties and the permeability of RPC, all of which contribute to RPC's durability.

1. The replacement of cement with UFS accelerated the early hydration speed of the cement. The TG test and the QXRD results indicated that the UFS' pozzolanic reactions increased, consuming large amounts of CH which improved the ITZ and blocked connected pores within the RPC. The MIP results showed a denser pore structure in the UFS sample than in SF sample.
2. RPC with high compressive strength can be obtained using OPC blended with either UFS or SF. The presence of steel fibres had a considerable effect on the mechanical properties of RPC.
3. The chloride permeability grade of the RPC when prepared using SF or UFS achieved a 'Very Low' status, which indicates that the RPC has good properties of the chloride resistance.

Acknowledgements This research is supported by the China Postdoctoral Science Foundation (2019M660037, 2020T130355).

References

1. Zhou M, Lu W, Song J, Lee GC. Application of ultra-high performance concrete in bridge engineering. Constr Build Mater. 2018;186:1256–67. https://doi.org/10.1016/j.conbuildmat.2018.08.036.
2. Alsalman A, Dang CN, Hale WM. Development of ultra-high performance concrete with locally available materials. Constr Build Mater. 2017;133:135–45. https://doi.org/10.1016/j.conbuildmat.2016.12.040.
3. Wang D, Wang Q, Huang Z. New insights into the early reaction of NaOH-activated slag in the presence of CaSO4. Compos Part B. 2020;198:108207. https://doi.org/10.1016/j.compositesb.2020.108207.
4. Wang Q, Wang D, Zhuang S. The soundness of steel slag with different free CaO and MgO contents. Constr Build Mater. 2017;151:138–46. https://doi.org/10.1016/j.conbuildmat.2017.06.077.

5. Dong Y. Performance assessment and design of ultra-high performance concrete (UHPC) structures incorporating life-cycle cost and environmental impacts. Constr Build Mater. 2018;167:414–25. https://doi.org/10.1016/j.conbuildmat.2018.02.037.
6. Wang C, Yang C, Liu F, Wan C, Pu X. Preparation of ultra-high performance concrete with common technology and materials. Cem Concr Compos. 2012;34:538–44. https://doi.org/10.1016/j.cemconcomp.2011.11.005.
7. Yu R, Song Q, Wang X, Zhang Z, Shui Z, Brouwers HJH. Sustainable development of ultra-high performance fibre reinforced concrete (UHPFRC): towards to an optimized concrete matrix and efficient fibre application. J Clean Prod. 2017;162:220–33. https://doi.org/10.1016/j.jclepro.2017.06.017.
8. Tayeh B, Bakar B, Johari M. Characterization of the interfacial bond between old concrete substrate and ultra-high performance fiber concrete repair composite. Mater Struct. 2013;46:743–53.
9. Chan Y, Chu S. Effect of silica fume on steel fiber bond characteristics in reactive powder concrete. Cem Concr Res. 2004;34:1167–72.
10. Richard P, Cheyrezy M. Composition of reactive powder concrexes. Cem Concr Res. 1995;25:1501–11.
11. Yanzhou P, Jun Z, Jiuyan L, Jin K, Fazhou W. Properties and microstructure of reactive powder concrete having a high content of phosphorous slag powder and silica fume. Constr Build Mater. 2015;101:482–7. https://doi.org/10.1016/j.conbuildmat.2015.10.046.
12. Richard P, Materiaux L, Bouygues G, Scientifique D. Water environment and nanostructural a reactive powder concrete network in reactive powder concrete. Cem Concr Compos. 1996;9465:23–9.
13. Yazıcı H, Yardımcı MY, Aydın S, Anıl S. Mechanical properties of reactive powder concrete containing mineral admixtures under different curing regimes. Constr Build Mater. 2009;23:1223–31. https://doi.org/10.1016/j.conbuildmat.2008.08.003.
14. Langan BW, Weng K, Ward MA. Effect of silica fume and fly ash on heat of hydration of Portland cement. Cem Concr Res. 2002;32:1045–51.
15. Ju Y, Tian K, Liu H, Reinhardt H, Wang L. Experimental investigation of the effect of silica fume on the thermal spalling of reactive powder concrete. Constr Build Mater. 2017;155:571–83. https://doi.org/10.1016/j.conbuildmat.2017.08.086.
16. Hafiz MA, Skibsted J, Denarié E. Influence of low curing temperatures on the tensile response of low clinker strain hardening UHPFRC under full restraint. Cem Concr Res. 2020;128:105940. https://doi.org/10.1016/j.cemconres.2019.105940.
17. Wu Z, Khayat KH, Shi C. Changes in rheology and mechanical properties of ultra-high performance concrete with silica fume content. Cem Concr Res. 2019;123:105786. https://doi.org/10.1016/j.cemconres.2019.105786.
18. Rao GA. Investigations on the performance of silica fume-incorporated cement pastes and mortars. Cem Concr Res. 2003;33:1765–70.
19. Wang Q, Wang D, Chen H. The role of fly ash microsphere in the microstructure and macroscopic properties of high-strength concrete. Cem Concr Compos. 2017;83:125–37. https://doi.org/10.1016/j.cemconcomp.2017.07.021.
20. Johari MAM, Brooks JJ, Kabir S, Rivard P. Influence of supplementary cementitious materials on engineering properties of high strength concrete. Constr Build Mater. 2011;25:2639–48. https://doi.org/10.1016/j.conbuildmat.2010.12.013.
21. Yu R, Spiesz P, Brouwers HJH. Development of an eco-friendly Ultra-High Performance Concrete (UHPC) with efficient cement and mineral admixtures uses. Cem Concr Compos. 2015;55:383–94.
22. Ganesh P, Murthy AR. Tensile behaviour and durability aspects of sustainable ultra-high performance concrete incorporated with GGBS as cementitious material. Constr Build Mater. 2019;197:667–80. https://doi.org/10.1016/j.conbuildmat.2018.11.240.
23. Teng S, Yang T, Lim D, Divsholi BS. Durability and mechanical properties of high strength concrete incorporating ultra fine Ground Granulated Blast-furnace Slag. Constr Build Mater. 2013;40:875–81. https://doi.org/10.1016/j.conbuildmat.2012.11.052.
24. GB/T 31387-2015, Reactive powder concrete. China. 2015.
25. ASTM. Standard Test Method for Electrical Indication of Concrete's Ability to Resist Chloride Ion Penetration, ASTM C1202. 100 Barr Harbor Drive. West Conshohocken, 6, 1997.
26. Ting L, Qiang W, Shiyu Z. Effects of ultra-fine ground granulated blast-furnace slag on initial setting time, fl uidity and rheological properties of cement pastes. Powder Technol. 2019;345:54–63. https://doi.org/10.1016/j.powtec.2018.12.094.
27. Ting L, Yuqi Z, Qiang W. Influence of ultra-fine slag and silica fume on properties of high-strength concrete. Mag Concr Res. 2020;72:610–21.
28. Mitchell DR, Hinczak I, Day R. Interaction of silica fume with calcium hydroxide solutions. Cem Concr Res. 1998;28:1571–84.
29. Rong ZD, Sun W, Xiao HJ, Wang W. Effect of silica fume and fly ash on hydration and microstructure evolution of cement based composites at low water: binder ratios. Constr Build Mater. 2014;51:446–50. https://doi.org/10.1016/j.conbuildmat.2013.11.023.
30. Liu J, Li Y, Ouyang P, Yang Y. Hydration of the silica fume-Portland cement binary system at lower temperature. Constr Build Mater. 2015;93:919–25. https://doi.org/10.1016/j.conbuildmat.2015.05.069.
31. Liu J, Guo R, Shi P, Huang L. Hydration mechanisms of composite binders containing copper slag at different temperatures. J Therm Anal Calorim. 2019;137:1919–28. https://doi.org/10.1007/s10973-019-08116-9.
32. Kuzielova E, Zemlicka M, Novotny R, Palou TM. Simultaneous effect of silica fume, metakaolin and ground granulated blast-furnace slag on the hydration of multicomponent cementitious binders. J Therm Anal Calorim. 2019;7:1527–37.
33. Wongkeo W, Thongsanitgarn P, Chaipanich CPA. Heat of hydration of cement pastes containing high-volume fly ash and silica fume. J Therm Anal Calorim. 2019;138:2065–75. https://doi.org/10.1007/s10973-019-08641-7.
34. Han J, Zhao M, Chen J, Lan X. Effects of steel fiber length and coarse aggregate maximum size on mechanical properties of steel fiber reinforced concrete. Constr Build Mater. 2019;209:577–91. https://doi.org/10.1016/j.conbuildmat.2019.03.086.
35. Wang X, Yuan J, Wei P, Zhu M. Effects of fly ash microspheres on sulfate erosion resistance and chlorion penetration resistance in concrete. J Therm Anal Calorim. 2020;139:3395–403. https://doi.org/10.1007/s10973-019-08705-8.